ORGANIC CHEMISTRY FRONTIERS

CCS 中国化学会 CHINESE CHEMICAL SOCIETY

SIOC 1950

ROYAL SOCIETY OF CHEMISTRY

RESEARCH ARTICLE

View Article Online
View Journal | View Issue

Cite this: *Org. Chem. Front.*, 2026, **13**, 2298

Electronic properties of diastereomeric Möbius shaped cyclotris[5]helicenes

Albert Artigas, †[a] Nicolas Vanthuyne, [b] Jean-Valère Naubron, [b,e] Denis Hagebaum-Reignier, [a] Yannick Carissan, [a] Maxime Rémond, ‡[c] Ludovic Favereau, [c,e] Harald Bock, [d,e] Fabien Durola *[d,e] and Yoann Coquerel *[a,e]

The in-depth analysis of the configurational, (chir)optical and aromatic properties of two diastereomeric singly and triply twisted Möbius-shaped macrocycles, the cyclotris[5]helicenes, in which three [5]helicene fragments with *like* and *unlike* helicity are connected by three C(sp^2)–C(sp^2) single bonds, led to the conclusion that global π electronic delocalization exists in these molecules. This was analyzed as a consequence of the reduced torsion angle (≤30°) at the C(sp^2)–C(sp^2) single bonds connecting the [5]helicene fragments. The enantiomers of both diastereomeric cyclotris[5]helicenes were thoroughly analyzed experimentally by unpolarized and circularly polarized vibrational, absorption and luminescence (fluorescence and phosphorescence) spectroscopies, all correlated with advanced DFT models, which provided insightful data on their S_0, S_1 and T_1 electronic states, and on their chirality. The theoretical analyses of aromaticity in both diastereomeric cyclotris[5]helicene macrocycles, as compared with recently reported analogues, confirmed their Möbius aromaticity.

Received 24th December 2025,
Accepted 9th February 2026

DOI: 10.1039/d5qo01741f

rsc.li/frontiers-organic

Introduction

With progress in organic synthesis, methods are now available for the property-driven design and reproducible precision synthesis of a variety of chiral polycyclic aromatic hydrocarbons (PAH). For instance, carbo[5]helicene units are now thought as elementary fragments to elaborate complex chiral shape-persistent π-conjugated chiral molecules, typically multi[5]helicenes[1] and macrocyclic cyclo[5]helicenes.[2] In this direction, Bock and Durola have developed the Perkin synthetic strategy,[3] which enabled the synthesis of many carboxyl-substituted polycyclic aromatic compounds with diverse shapes, and notably various [5]helicene-containing macrocyclic molecules: the figure-eight cyclobis[5]helicene **1**,[4] the triply[5]helicene-bridged(1,3,5)cyclophane **2**,[5] and the diastereomeric, triply and singly twisted Möbius-shaped[6] cyclotris[5]helicenes $\boldsymbol{D_3}$-**3** and $\boldsymbol{C_2}$-**3** (Fig. 1).[7] In these macrocycles, two or three [5]helicene fragments are linked by C(sp^2)–C(sp^2) biphenyl-like single bonds (with a phenyl tether for **2**). In principle, because there is no substituent at any *ortho* position around these biphenyl-like single bonds, free rotation around these bounds may be expected at 298 K. However, the mechanical constraint

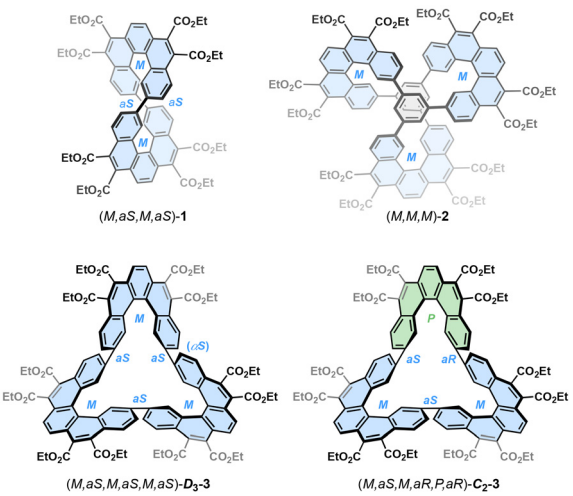

Fig. 1 Macrocyclic cyclo[5]helicenes synthesized through the Perkin strategy by the Durola group.

[a]*Aix Marseille Univ, CNRS, Centrale Med, ISM2, 13397 Marseille, France. E-mail: yoann.coquerel@univ-amu.fr*
[b]*Aix Marseille Univ, CNRS, Centrale Med, FSCM, 13397 Marseille, France*
[c]*Univ Rennes, CNRS, ISCR-UMR 6226, 35000 Rennes, France*
[d]*Centre de Recherche Paul Pascal, CNRS & Univ. Bordeaux, 33600 Pessac, France. E-mail: fabien.durola@crpp.cnrs.fr*
[e]*Centre National de la Recherche Scientifique, CNRS, 75016 Paris, France*
†Current address: Institut de Química Computacional i Catàlisi (IQCC) and Departament de Química, Universitat de Girona (UdG), Facultat de Ciències, Girona, Catalunya 17003, Spain.
‡Current address: Univ Angers, CNRS, MOLTECH-Anjou, SFR MATRIX, 49000 Angers, France.

induced by the spatial arrangement of the [5]helicene fragments impedes free rotation around the biphenyl-like single bonds, which make these molecule shape-persistent. The direct consequence of this is that some of these biphenyl-like single bonds are stereogenic due to atropisomerism. For instance, it was previously analysed in **1** having two (*M*)-configured [5]helicene fragments that both single bonds are blocked in the (*aS*)-configuration.[8] Thus, a complete stereochemical description of **1** according to Cahn–Ingold–Prelog (CIP) rules is (*M*,*aS*,*M*,*aS*)-**1** for the depicted enantiomer in Fig. 1 [and (*P*,*aR*,*P*,*aR*)-**1** for the other enantiomer]. Similarly, cyclotris[5]helicenes ***D*$_3$-3** embeds six stereogenic elements: three helices and three axes, and the complete stereochemical description of its depicted enantiomer in Fig. 1 is (*M*,*aS*,*M*,*aS*,*M*,*aS*)-***D*$_3$-3** [and (*P*,*aR*,*P*,*aR*,*P*,*aR*)-***D*$_3$-3** for the other enantiomer]. For its diastereomer ***C*$_2$-3**, application of the CIP nomenclature for the depicted enantiomer in Fig. 1 results in (*M*,*aS*,*M*,*aR*,*P*,*aR*)-***C*$_2$-3** [and (*P*,*aR*,*P*,*aS*,*M*,*aS*)-***C*$_2$-3** for the other enantiomer]. The single bond in the triply[5]helicene-bridged(1,3,5)cyclophane **2** are not stereogenic due to CIP equivalence at both sides of the central phenyl ring, a stereochemical fact not yet revealed about this molecule.

The existence of torsion angles at the single bonds between the [5]helicenyl moieties in **1** and **3**, and between the phenyl and the [5]helicenyl moieties in **2**, raises the question: are these molecules globally π-conjugated, with ring-to-ring π electrons delocalization across the single bonds? There is no simple yes or no answer to this question because: (i) it depends largely on the torsion angles at each single bond, (ii) multiple delocalization circuits, with local, semi-local and global character, can develop in these molecules, and (iii) strictly speaking, pure σ and π systems no longer exist in these contorted molecules as they overlap (and overlap differently on both faces of each ring), and it may be preferable to invoke π-type conjugation rather than just π conjugation for contorted molecules. For clarity, only π conjugation is referred to as herein, with the understanding it is an (acceptable) approximation. We and others have previously attempted to answer the question of global π conjugation for molecules **1** and **2**: figure-eight **1** was found not a globally π conjugated molecule, *i.e.*, with two separated 22-electron π systems, while a 78-electron π global delocalization circuit was found to exist in cyclophane **2**, albeit of minor intensity compared to other delocalization circuits operating in this molecule.[5,9] For the macrocyclic triply twisted Möbius-shaped molecule ***D*$_3$-3**, previous investigations indicated that electronic delocalisation circuits exist at its edges: a 48-electron Möbius aromatic system located at the external edge with mainly a π character, and a 24-electron anti-aromatic circuit located at the internal edge with a pronounced σ character.[7] In this article, we provide complementary analyses of the electronic π delocalization in both diastereomers of the Möbius-shaped molecules **3**, now using an isotropic magnetic criterion, the 3DIMS (three-dimensional isotropic magnetic shielding) analysis,[10] and an electronic criterion, the EDDB (electron density of delocalized bonds) analysis,[11] which confirmed their Möbius aromaticity.

A highly sought-after property of shape-persistent chiral π-conjugated molecules is their emission of circularly polarized luminescence (CPL) with potentially large dissymmetry factors $|g_{lum}|$.[12] Maximal dissymmetry factors in molecules can be expected when their electric and magnetic transition moments are parallel or antiparallel one to another. For instance, the D_2 point group symmetric figure-eight compound **1** shows a relatively high dissymmetry factor $|g_{lum}| = 5 \times 10^{-3}$ (at its maximum of fluorescence at 447 nm) for a molecular organic CPL emitter, *ca.* a 35 fold enhancement when compared to carbo[6]helicene.[8] More recently, some figure-eight arylophane analogs of **1**, *i.e.*, with small aryl tethers (1,4-phenyl, 2,6-naphthyl, 2,6-anthracenyl, 2,7-pyrenyl or 3,10-perylenyl) between the two [5]helicene fragments, exhibited a range of dissymmetry factors $|g_{lum}| = 0.19–38 \times 10^{-3}$.[2c,f] Lately, some analogs of Möbius-shaped cyclotris[5]helicenes ***D*$_3$-3** and ***C*$_2$-3** embedding small aryl tethers (1,4-phenyl, 2,6-naphthyl or 2,7-pyrenyl) between the three [5]helicene fragments have shown comparable $|g_{lum}|$ in the range $0.75–1.2 \times 10^{-3}$ for the D_3 point group symmetric diastereomers, and $0.20–1.3 \times 10^{-3}$ for the C_2 point group symmetric diastereomers.[2f] These molecular dissymmetry factors, however, remain modest when compared to the nearly maximum dissymmetry factors that can be obtained from chiral luminescent materials, *i.e.*, 2 for a total left or right CPL.[13] In this article, we report the resolution of the enantiomers of both diastereomers of the Möbius-shaped cyclotris[5]helicenes ***D*$_3$-3** and ***C*$_2$-3** by semi-preparative HPLC on chiral stationary phases, their chiroptical properties including optical rotation dispersion at discrete wavelengths, VCD (vibrational circular dichroism), ECD (electronic circular dichroism) and CPL spectroscopies, and the examination of their conformational behavior by experimental and computational methods.

Results and discussion

Racemic samples of the Möbius-shaped cyclotris[5]helicenes ***D*$_3$-3** and ***C*$_2$-3** were obtained in equivalent amounts from the photocyclization of a macrocyclic precursor as previously described.[7] The resolution of the enantiomers of ***D*$_3$-3** and ***C*$_2$-3** was achieved through semi-preparative HPLC (see details in section S1 in the SI). From a 46 mg sample of racemic ***D*$_3$-3** contaminated by minor products using a Chiralpak IE column (250 × 10 mm) eluted with heptane/ethanol/dichloromethane (5 : 3 : 2), 8 mg of the first eluted enantiomer (rt = 7.44 min) and 11 mg of the second eluted enantiomer (rt = 9.30 min) were obtained (note: +27 mg recovered mixture) both with >99.5% ee. Similarly, now using a Chiralpak ID (250 × 10 mm) column eluted with heptane/ethanol/dichloromethane (5 : 3 : 2), 47 mg of material containing essentially racemic ***C*$_2$-3** afforded 12 mg of the first eluted enantiomer (rt = 5.57 min) with >98% ee and 14 mg of the second eluted enantiomer (rt = 7.86 min) with >98.5% ee (note: +21 mg recovered mixture). The absolute configurations of the enantiomers of ***D*$_3$-3** and ***C*$_2$-3** were determined by VCD and ECD spectroscopies

(*vide infra*), comparing their experimental and simulated spectra (Fig. 3 and 4). The enantiomers of both compounds displayed mirror-image spectra, and it could be safely concluded that the first eluted enantiomers are (*P*,*aR*,*P*,*aR*,*P*,*aR*)-***D*$_3$-3** (rt = 7.44 min) and (*M*,*aS*,*M*,*aR*,*P*,*aR*)-***C*$_2$-3** (rt = 5.57 min), respectively.

A solution of (*M*,*aS*,*M*,*aR*,*P*,*aR*)-***C*$_2$-3** (>98% ee) was heated in boiling ethanol (bp = 78.4 °C) and the enantiomers ratio was monitored by chiral HPLC overtime (see details in section S2 in the SI). A clean enantiomerization was observed, which allowed to determine experimentally the barrier to enantiomerization of ***C*$_2$-3** at $\Delta G^{\ddagger}_{enant}$ = 114.4 kJ mol^{-1} (at 78.4 °C in ethanol). This $\Delta G^{\ddagger}_{enant}$ value indicates that enantiopure ***C*$_2$-3** is chemically stable at 78 °C, and that it can racemize at a significant rate at temperatures above room temperature. In contrast, heating a 1,2,4-trichlorobenzene solution of (*P*,*aR*,*P*,*aR*,*P*,*aR*)-***D*$_3$-3** (>99.5% ee) at 214 °C for 24 h did not allow to evidence any change by chiral HPLC, indicating both its chemical and conformational stability at 214 °C, and that the barrier to diastereomers interconversion ***D*$_3$-3** → ***C*$_2$-3** is higher than 183 kJ mol^{-1}.

Using DFT methods at the SMD(ethanol)-D3(BJ)-B3LYP/6-311G(d,p)//SMD(ethanol)-B3LYP/6-311G(d,p) level of theory at 351.5 K, it was determined that ***C*$_2$-3** is the more stable diastereomer, with a relative Gibbs energy of ***D*$_3$-3** found at ΔG = 25.8 kJ mol^{-1} (Fig. 2). Notably, as previously identified,[7] the inclusion of a dispersion correction term, namely D3(BJ),[14] is crucial to analyze the relative stability of ***C*$_2$-3** and ***D*$_3$-3** (see details in section S3 in the SI, Fig. S1 and S2). The conversion of the less stable diastereomer ***D*$_3$-3** into the thermodynamic diastereomer ***C*$_2$-3** would require to surmount a barrier of $\Delta G^{\ddagger}_{dia}$ > 200 kJ mol^{-1} (*via* **TS$_1$**), indicating it is shape-persistent at temperatures below 200 °C. Examination of the enantiomerization of ***C*$_2$-3** confirmed it is a single step process occurring *via* **TS$_2$**, requiring the inversion of configuration of only one [5]helicene fragment, with a barrier to enantiomerization computed at $\Delta G^{\ddagger}_{enant}$ = 137.4 kJ mol^{-1} (at 78.4 °C). Yet consistent with the experimental value, the computed value of $\Delta G^{\ddagger}_{enant}$ for ***C*$_2$-3** is somewhat over-estimated (by 23.0 kJ mol^{-1}). A plausible reason for this deviation (20% over-estimation) is it was not possible to identify the corresponding transition state using the D3(BJ) dispersion correction scheme in the calculations (see discussion in section S3 in the SI). A noticeable fact about the enantiomerization of ***C*$_2$-3**, a chiral molecule that contains three stereogenic [5]helicene fragments, is that the inversion of configuration of a single of its [5]helicene fragments leads to a net enantiomerization of the entire molecule. Comparing the experimentally determined enantiomerization barriers of ***C*$_2$-3** ($\Delta G^{\ddagger}_{enant}$ = 114.4 kJ mol^{-1} at 351.5 K) and [5]helicene itself ($\Delta G^{\ddagger}_{enant}$ = 98.3 kJ mol^{-1} at 304–320 K (ref. 15)), notwithstanding the ester substituents, indicated that the rigid chiral environment in ***C*$_2$-3** surprisingly leads to only a modest increase in the barrier.

As a first chiroptical analysis, the optical rotation dispersions (ORD) of the enantiomers of ***D*$_3$-3** and ***C*$_2$-3** were measured at several discrete wavelengths as summarized in Table 1. The increasing magnitude of the optical rotations at increasingly energetic wavelengths, from 589 nm to 546 nm, is a standard phenomenon for comparable molecules,[4,5] and no attempt was made to rationalize the sign and amplitude of these values at this stage. For (*P*,*aR*,*P*,*aR*,*P*,*aR*)-***D*$_3$-3**: $[\alpha]^{25}_{D}$ = +1850 ° mL g^{-1} (dichloromethane, *c* = 0.114), and for (*P*,*aR*,*P*,*aS*,*M*,*aS*)-***C*$_2$-3**: $[\alpha]^{25}_{D}$ = ° mL g^{-1} dm^{-1} −900 (dichloromethane, *c* = 0.105).

The experimental IR and VCD spectra of both ***D*$_3$-3** and ***C*$_2$-3**, together with the simulated spectra for (*P*,*aR*,*P*,*aR*,*P*,*aR*)-***D*$_3$-3** and (*P*,*aR*,*P*,*aR*,*M*,*aS*)-***C*$_2$-3** computed at the SMD(CH_2Cl_2)-B3LYP/6-311G(d,p) level of theory, are shown in Fig. 3 (see also section S4 in the SI, Fig. S4 and S5). The calculated spectra reproduce well the main features of the experimental data for the first eluted enantiomer of ***D*$_3$-3** and the second eluted enantiomer of ***C*$_2$-3**, respectively. In particular, the VCD spectra exhibit clear differences at 1300 and 1267 cm^{-1}, corresponding to negative and positive C_{ar}–H deformation bands, respectively, which are accurately reproduced by the simulations. These modes are delocalized over the three cyclotris[5]helicene units rather than localized on a single subunit. For ***D*$_3$-3**, which contains three [5]helicene fragments of *like* helicity, these deformation bands are significantly more intense than in ***C*$_2$-3**, where *unlike* helicities reduce their amplitude. In both (*P*,*aR*,*P*,

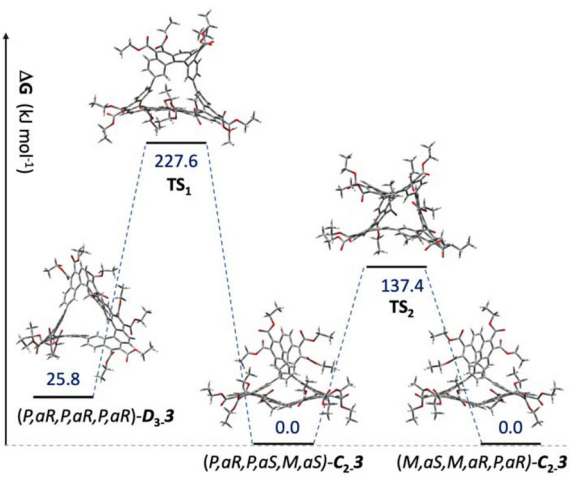

Fig. 2 Computational conformational analysis of cyclotris[5]helicenes ***D*$_3$-3** and ***C*$_2$-3** using DFT. Gibbs energies in kJ mol^{-1} computed at 351.52 K at the SMD(ethanol)-B3LYP-D3(BJ)/6-311G(d,p)//SMD(ethanol)-B3LYP/6-311G(d,p) level of theory.

Table 1 Optical rotation dispersions of the enantiomers of ***D*$_3$-3** and ***C*$_2$-3** measured at several discrete wavelengths in dichloromethane (*c* = 0.114, 0.135, 0.105, and 0.150 from top to bottom). Values are given in ° mL g^{-1} dm^{-1}

	$[\alpha]^{25}_{589}$	$[\alpha]^{25}_{578}$	$[\alpha]^{25}_{546}$
(*P*,*aR*,*P*,*aR*,*P*,*aR*)-***D*$_3$-3**	+1850	+2000	+2500
(*M*,*aS*,*M*,*aS*,*M*,*aS*)-***D*$_3$-3**	−1850	−2000	−2500
(*P*,*aR*,*P*,*aR*,*M*,*aS*)-***C*$_2$-3**	−900	−975	−1250
(*M*,*aS*,*M*,*aS*,*P*,*aR*)-***C*$_2$-3**	+900	+975	+1250

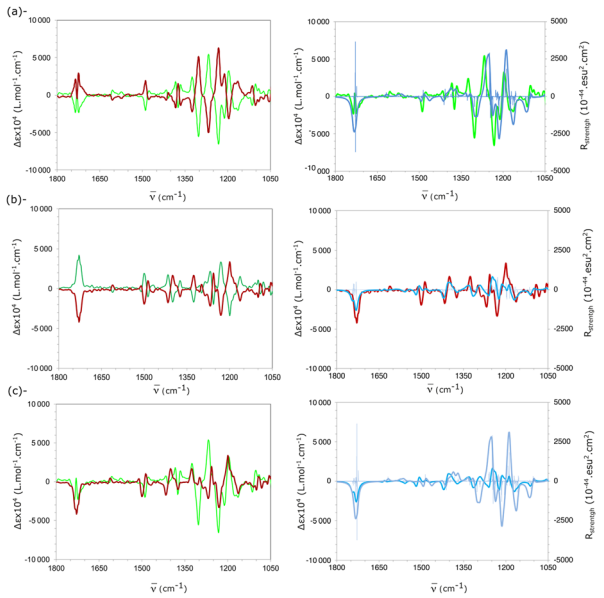

Fig. 3 VCD spectra of (a) D_3-3 and (b) C_2-3 recorded in CD_2Cl_2. Green (light and dark): first-eluted enantiomers; red (light and dark): second-eluted enantiomers; blue (light and dark): calculated for (*P*,*aR*,*P*,*aR*,*P*,*aR*)-D_3-3 and (*P*,*aR*,*P*,*aS*,*M*,*aS*)-C_2-3, using the SMD(CH_2Cl_2)-B3LYP/6-311G(d,p) level of theory. (c) Overlay of experimental VCD spectra of first-eluted D_3-3 and second-eluted C_2-3, and calculated VCD spectra of (*P*,*aR*,*P*,*aR*,*P*,*aR*)-D_3-3 and (*P*,*aR*,*P*,*aS*,*M*,*aS*)-C_2-3.

aR,*P*,*aR*)-D_3-3 and (*P*,*aR*,*P*,*aS*,*M*,*aS*)-C_2-3, the VCD band associated with the C=O stretching vibration of the ethyl ester groups exhibits a negative sign, indicating that this mode is largely insensitive to the [5]helicene stereogenicity. The consistent agreement between experimental and computed IR/VCD spectra, including the sign and relative intensity of diagnostic bands, unambiguously supports the assignment of the absolute configurations as (*P*,*aR*,*P*,*aR*,*P*,*aR*)-D_3-3 for the first-eluted enantiomer and (*P*,*aR*,*P*,*aS*,*M*,*aS*)-C_2-3 for the second-eluted enantiomer.

An intriguing feature of D_3-3 and C_2-3 lies in their extended π-electron delocalization, potentially expanding across the three [5]helicene units, which governs their photophysical and chiroptical electronic responses in the UV-vis region of the electromagnetic spectrum. These properties are determined by the balance between the electric and magnetic transition dipole moments, and thus depend critically on the electronic coupling between the helicenic subunits and their relative (*M*) or (*P*) configurations.[16] In the present systems, this structure–property relationship can be rationalized both experimentally and theoretically, as D_3-3 contains three [5]helicene fragments of identical configuration (*like* relationship) while C_2-3 contains one [5]helicene fragment of opposite configuration relative to the two others (*unlike* relationship). The UV-vis absorption spectra of both macrocyclic compounds have been previously investigated, and compared to the reference tetraethyl ester [5]helicene fragment.[7] This first comparative characterization of D_3-3 and C_2-3 clearly evidences an electronic interaction between the helicene subunits, which is highlighted by a 75 nm bathochromic-shift in the onset of their UV–vis spectra (onset at 450 nm) relative to the reference tetraethyl ester [5]helicene fragment (onset at 375 nm). Further insights into the effect of helicene configuration within these macrocycles were obtained from electronic circular dichroism (ECD) measurements (Fig. 4, see also Fig. S6 and S7 in the SI). As expected, the enantiomers of both D_3-3 and C_2-3 display mirror-image ECD spectra, although with marked differences between the diastereomers. For instance, the ECD response of (*P*,*aR*,*P*,*aR*,*P*,*aR*)-D_3-3 comprises: (i) a positive band at 200 nm ($\Delta\varepsilon \approx +180$ M^{-1} cm^{-1}), (ii) a strong negative band at 230 nm ($\Delta\varepsilon \approx -300$ M^{-1} cm^{-1}), (iii) an intense bisignate signal with extrema at 270 and 300 nm ($|\Delta\varepsilon| \approx 410$ M^{-1} cm^{-1}), (iv) a broad positive band at 360 nm ($\Delta\varepsilon \approx +400$ M^{-1} cm^{-1}) with a shoulder at 340 nm, and (v) a weak negative band at 405 nm ($\Delta\varepsilon \approx -50$ M^{-1} cm^{-1}). In contrast, (*P*,*aR*,*P*,*aS*,*M*,*aS*)-C_2-3 exhibits a weaker overall intensity, along with additional positive/negative features between 220 and 340 nm. This spectral region typically reflects the ^1B_a and ^1B_b transitions characteristic of carbohelicenes,[17] highlighting the strong influence of the (*M*)/(*P*) relative configuration in the chiroptical response. The simulation of the UV-vis and ECD spectra of both D_3-3 and C_2-3 by TD-DFT methods well reproduced their experimental spectra, which confirmed the absolute configurations of the samples as deduced from their VCD spectroscopy analyses. In line with these observations, the absorption dissymmetry factors ($|g_{abs}|$) at 405 nm reach 4.0×10^{-3} for D_3-3 and 3.3×10^{-3} for C_2-3,

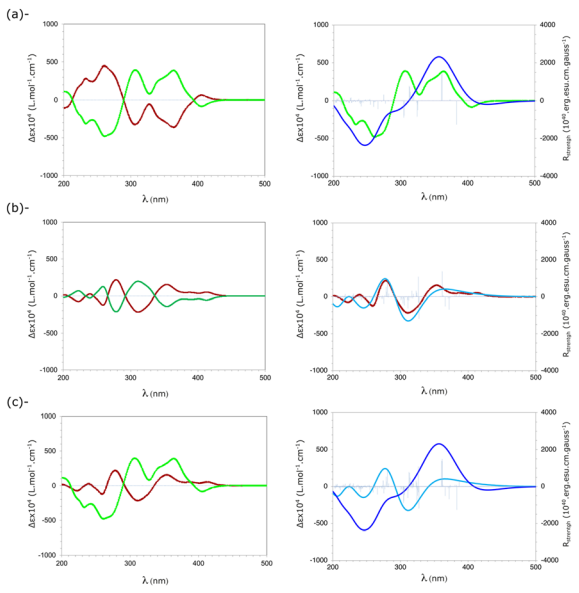

Fig. 4 ECD spectra of (a) D_3-3 and (b) C_2-3 recorded in acetonitrile. Green (light and dark): first-eluted enantiomers; red (light and dark): second-eluted enantiomers; blue (light and dark) calculated for (*P*,*aR*,*P*,*aR*,*P*,*aR*)-D_3-3 and (*P*,*aR*,*P*,*aS*,*M*,*aS*)-C_2-3, using the SMD(acetonitrile)-CAM-B3LYP/Def2SVP//B3LYP/6-311G(d,p) level of theory. (c) Overlay of experimental ECD spectra of first-eluted D_3-3 and second-eluted C_2-3, and calculated ECD spectra of (*P*,*aR*,*P*,*aR*,*P*,*aR*)-D_3-3 and (*P*,*aR*,*P*,*aS*,*M*,*aS*)-C_2-3.

values comparable with those reported for other [5]helicene-based Möbius-shaped macrocycles.[2f]

Interestingly, the sign of the lowest-energy ECD band (390–430 nm) is inverted between (*P*,*aR*,*P*,*aR*,*P*,*aR*)-***D*$_3$-3** and (*P*,*aR*,*P*,*aS*,*M*,*aS*)-***C*$_2$-3**, despite comparable intensity. This inversion suggests that all helicene units contribute significantly to the frontier molecular orbitals (FMO) in both macrocycles. Examination of the FMO revealed that the HOMO and HOMO−1, and the LUMO and LUMO+1 of ***D*$_3$-3** are degenerated, with equivalent electronic density of each [5]helicene fragments, which is expected form the molecular symmetry (Fig. 5a). In contrast, the FMO of ***C*$_2$-3** are, as expected, close in energy but not degenerated (Fig. 5b): the HOMO−1 is mostly localized over the [5]helicene fragment of *unlike* configuration, the HOMO is predominately delocalized on the two [5]helicene fragments of *like* configuration, the LUMO is delocalized over two [5]helicene fragments of *unlike* configurations, and the LUMO+1 is mostly localized over one [5]helicene fragment of *like* configuration. The lowest-energy band in the ECD spectrum of (*P*,*aR*,*P*,*aR*,*P*,*aR*)-***D*$_3$-3**, corresponding to the $S_0 \rightarrow S_1$ transition, is negatively signed. In contrast, the lowest-energy band in the ECD spectrum of (*P*,*aR*,*P*,*aS*,*M*,*aS*)-***C*$_2$-3** is positively signed. The FMO distribution shown in Fig. 5 helps rationalizing these opposite signs: in both macrocycles the $S_0 \rightarrow S_1$ transitions arise mainly from HOMO−1 → LUMO and HOMO → LUMO+1 contributions. However, in ***C*$_2$-3** it is dominated by the [5]helicene fragment of *unlike* configuration, leading to the inversion of the sign of the lowest ECD band.

The influence of the relative configurations of the [5]helicene fragments in ***D*$_3$-3** and ***C*$_2$-3** is modestly reflected in their emissive properties (Fig. 6, see section S5 in the SI for details). In solution in three solvents of different polarity (toluene, dichloromethane and acetonitrile), both compounds show broad emission with maxima at 465 nm (for ***C*$_2$-3**) and 450 nm (for ***D*$_3$-3**), comparable to the parent tetraethyl ester [5]helicene (with maximum at 457 nm, see Fig. S8 in the SI). The photoluminescence quantum yields are modest (Φ_{PL} = 14% for ***D*$_3$-3** and Φ_{PL} = 17% for ***C*$_2$-3**) with fluorescence lifetimes of 5.5 ns for both compounds, consistent with the efficient intersystem crossing generally observed in carbohelicenes and other distorted aromatic molecules.[18] At 77 K in frozen 2-MeTHF matrix, both compounds exhibit dual emission: a structured fluorescence between 420–515 nm, and a lower-energy phosphorescence between 560–760 nm, with a long lifetime of *ca.* 0.5–0.6 s. The time-gated measurements (middle of Fig. 6c, see also Fig. S12 in the SI) unambiguously isolated the phosphorescence, which is red-shifted relative to the parent tetraethyl ester [5]helicene fragment (onset at 525 nm), indicating that the ***D*$_3$-3** and ***C*$_2$-3** multihelicenic frameworks stabilizes the triplet states more efficiently than the singlet ones (onsets at 550 nm). The luminescence properties of ***D*$_3$-3**, ***C*$_2$-3** and the parent [5]helicene were simulated using time-dependent DFT and a path integral approach for the dynamics[19] as implemented in ORCA 6.1.[20] However, to avoid prohibitive calculation costs, it was judged necessary to reduce the size of the systems, *i.e.*, using their stripped-down versions without the ester substituents (with 'only' 102 atoms *vs.* 210 atoms for the full systems). The calculated spectra reproduce very well the two peaked vibronic bands at 440 and 470 nm as well as the shoulder at 500 nm, originating from the S_1 vibronic states. The phosphorescence spectra display two bands at 590 and 645 nm, originating from the T_1 vibronic states. Notably, it was necessary to include the D4 dispersion correction scheme[21] in the calculations for the calculated energies to match the experimental ones. In both fluorescence and phosphorescence spectra, it is interesting to note that more than 99% of the

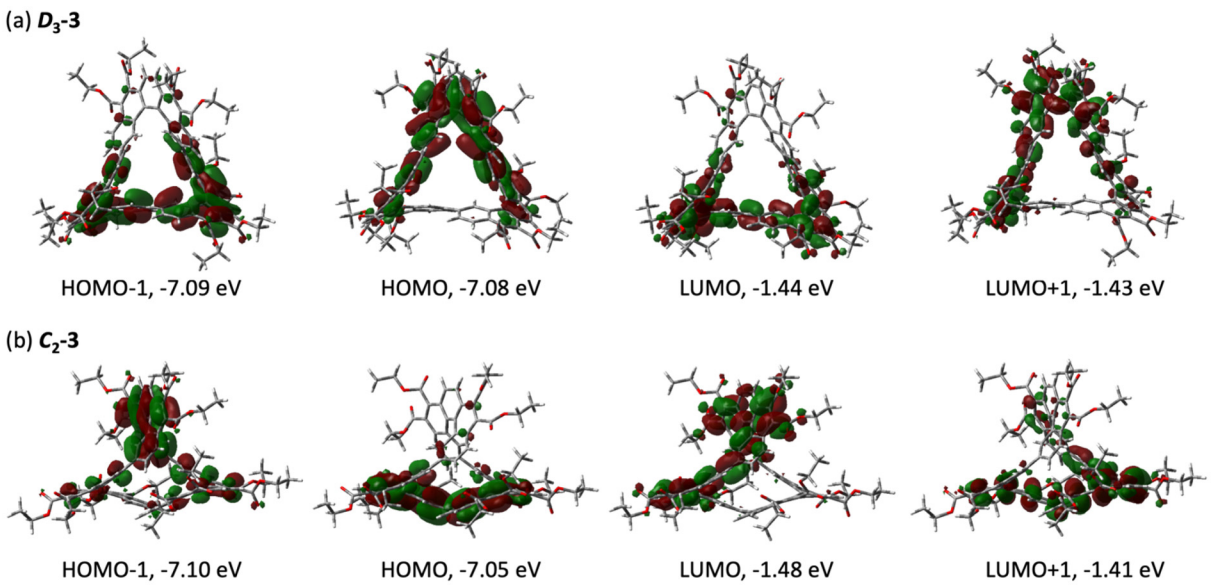

Fig. 5 Frontier molecular orbitals (FMO) of (a) ***D*$_3$-3** and (b) ***C*$_2$-3**, calculated at the SMD(acetonitrile)-CAM-B3LYP/Def2SVP//B3LYP/6-311G(d,p) level of theory.

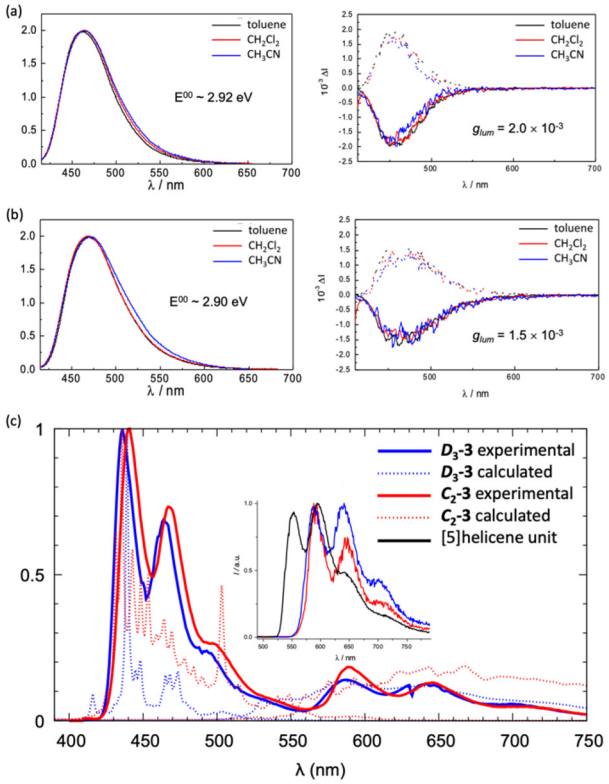

Fig. 6 (a) Fluorescence and CPL profiles of (*P*,*aR*,*P*,*aR*,*P*,*aR*)-***D*$_3$-3** (solid lines) and (*M*,*aS*,*M*,*aS*,*M*,*aS*)-***D*$_3$-3** (dashed lines) in toluene, dichloromethane and acetonitrile (λ_{ex} = 395 nm for fluorescence, λ_{ex} = 350 nm for CPL). (b) Fluorescence and CPL profiles of (*M*,*aS*,*M*,*aR*,*P*,*aR*)-***C*$_2$-3** (solid lines) and (*P*,*aR*,*P*,*aS*,*M*,*aS*)-***C*$_2$-3** (dashed lines) in toluene, dichloromethane and acetonitrile (λ_{ex} = 395 nm for fluorescence, λ_{ex} = 350 nm for CPL). (c) Normalized fluorescence and phosphorescence spectra of ***D*$_3$-3** and ***C*$_2$-3** in a frozen 2-MeTHF matrix at 77 K; the calculated spectra were obtained using the B3LYP-D4/def2-TZVP level of theory; the time-gated experimental measurements isolating phosphorescence are incrusted.

band intensities are due to the vibronic coupling (Herzberg-Teller or HT effect), the Franck–Condon intensities being at most four orders of magnitude smaller than the HT intensities for the fluorescence and two orders of magnitude smaller than the HT intensities for the phosphorescence. The adiabatic energy differences (ZPE corrected) between the S_0, S_1 and T_1 states for ***D*$_3$-3**, ***C*$_2$-3** and the parent [5]helicene fragment are reported in Table 2. Both the S_0–S_1 and S_0–T_1 excitation energies decrease from the parent [5]helicene fragment to the cyclotris[5]helicenes ***D*$_3$-3** and ***C*$_2$-3**, which aligns with the red shift observed in the experimental fluorescence and phosphorescence spectra.

Table 2 S_1 and T_1 ZPE corrected adiabatic energy differences relative to the S_0 state calculated in eV (B3LYP-D4/Def2-SVP level) and experimental luminescence onset energies for ***D*$_3$-3**, ***C*$_2$-3** and the parent tetraethyl ester [5]helicene

	S_1 (eV)	T_1 (eV)
***D*$_3$-3** calculated	2.98	2.24
***C*$_2$-3** calculated	2.86	2.17
***D*$_3$-3** and ***C*$_2$-3** experimental	2.93	2.36
Parent [5]helicene calculated	3.15	2.39
Parent [5]helicene experimental	3.02	2.19

The spin density maps and the 3DIMS maps[10] of the T_1 states of both ***D*$_3$-3** and ***C*$_2$-3** are shown in Fig. 7. Interestingly, the excess of α spin densities corresponds to regions where the 3DIMS maps of the respective T_1 states display negative values of the magnetic shielding, corresponding to semi-local paratropic currents, *i.e.*, semi-local antiaromaticity, but of different intensities: strong for ***D*$_3$-3** and weak for ***C*$_2$-3**. In the case of the T_1 state of ***D*$_3$-3**, the excess of α spin density is localized on a single [5]helicene fragment in which a semi-local 22 π electrons antiaromatic paratropic current can easily develop. This is consistent with Baird's rule which states that the T_1 state of a 4n + 2π electron system should be antiaromatic. In contrast, in the T_1 state of ***C*$_2$-3**, the excess of α spin density is localized over two halves of two [5]helicene fragments connected by a single bond, which impedes the formation of a large and intense semi-local antiaromatic paratropic current, resulting in a semi-local non aromatic (actually just slightly antiaromatic) character visible on the corresponding 3DIMS map.

The CPL spectra of the enantiopure (>98% ee) samples of ***D*$_3$-3** and ***C*$_2$-3** were recorded in three solvents of different polarity (toluene, dichloromethane and acetonitrile). Negligible solvent effects were observed, indicating the absence of charge-transfer character in the low-energy transitions, which is consistent with the calculated π → π* transitions of the FMO. For both ***D*$_3$-3** and ***C*$_2$-3**, mirror-image responses were observed with maxima corresponding with those of the non-polarized spectra. The $|g_{lum}|$ values reach 2.0

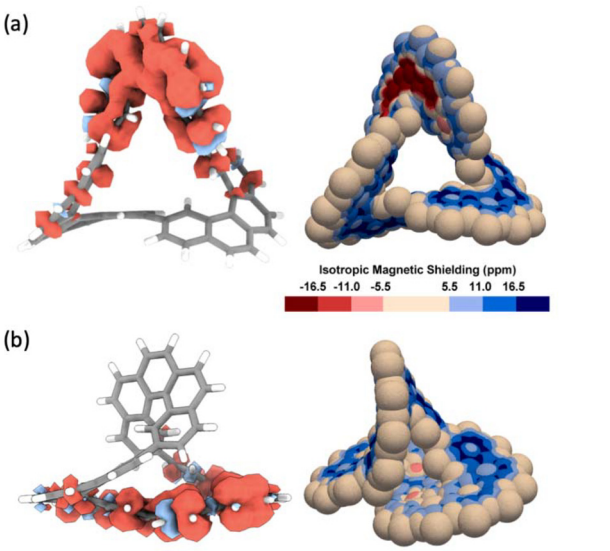

Fig. 7 Spin density maps (left) and 3DIMS maps (right) of the T_1 states at the geometry of the S_0 state for (a) ***D*$_3$-3** and (b) ***C*$_2$-3**. In the spin density maps, the red color corresponds to an excess of α spin density, the blue color corresponds to an excess of β spin density.

$\times 10^{-3}$ for ***D*$_3$-3** and 1.5×10^{-3} for ***C*$_2$-3**, in line with typical good organic CPL emitters, higher than the recently reported $|g_{lum}|$ values for some [5]helicene-based Möbius arylophanes.[2f] A notable constitutional difference between Möbius-shaped ***D*$_3$-3** and ***C*$_2$-3** discussed herein and other [5]helicene-based Möbius-shaped arylophanes is that in ***D*$_3$-3** and ***C*$_2$-3** no or very limited free rotation is allowed at the C(sp^2)–C(sp^2) biphenyl-like single bonds, unlike in other comparable molecules. Our findings suggest that restricting internal rotation around the C(sp^2)–C(sp^2) biphenyl-like linkages with torsion angles in the magnitude of 30° or less is a promising strategy to enhance CPL intensity in semi-condensed multihelicenic architectures.[22] The CPL brightness ($B_{CPL} = \varepsilon \times \Phi_{PL} \times |g_{lum}|/2$)[23] for ***D*$_3$-3** and ***C*$_2$-3** were determined to be 3.6 and 2.4 M^{-1} cm^{-1}, respectively, as a result of their modest molar extinction coefficients and modest emission quantum yields; nevertheless these values of B_{CPL} are state-of-the-art values for multicarbo [n]helicenes (typically <1 M^{-1} cm^{-1}).[24]

Analyzing magnetically-induced current densities (MICD, an anisotropic vectorial criterion of aromaticity) and their an-

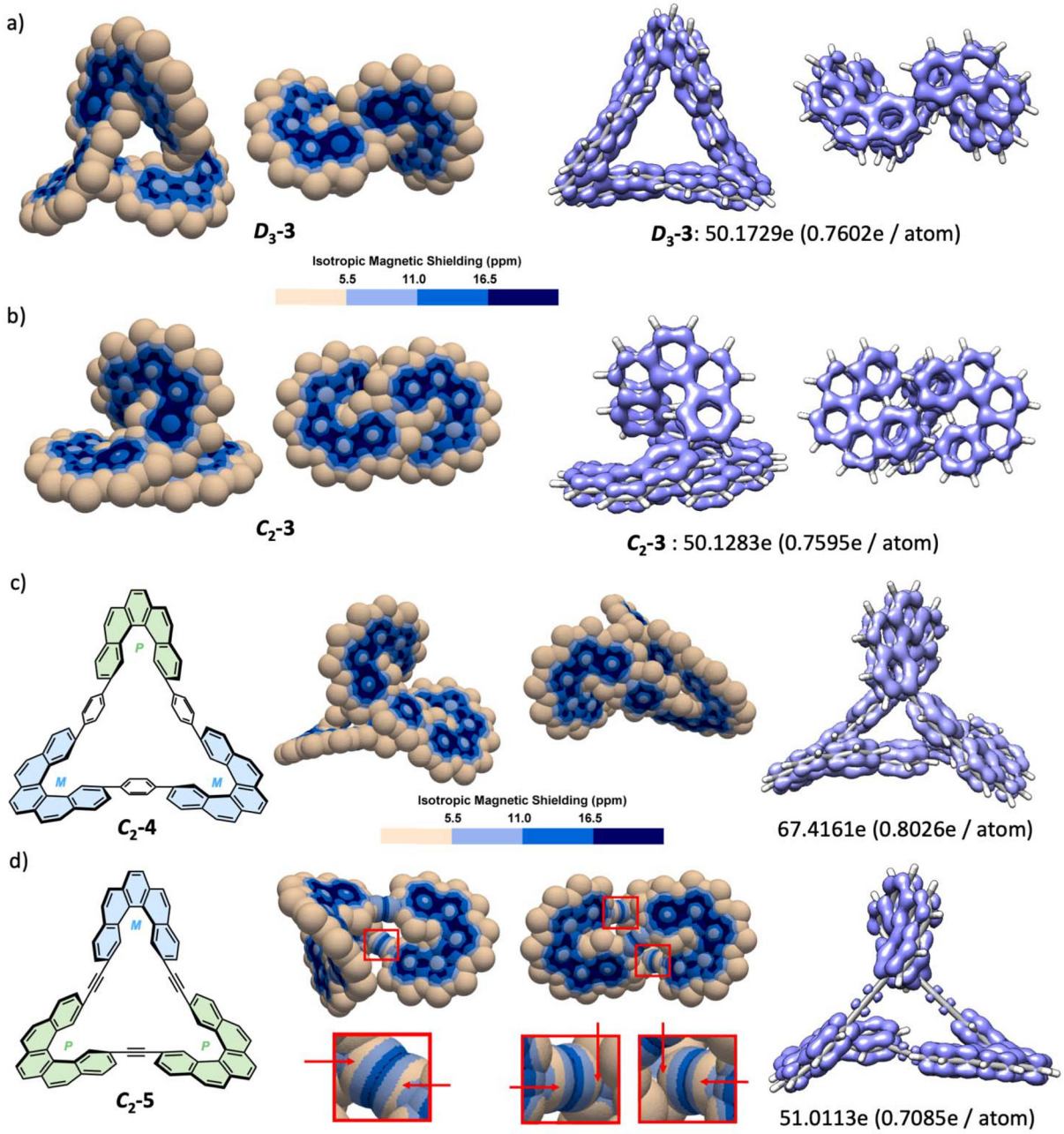

Fig. 8 (a) 3DIMS maps and EDDB$_H$(r) plots (isovalue = 0.02) of (*M*,*M*,*M*)-***D*$_3$-3**. (b) 3DIMS maps and EDDB$_H$(r) plots (isovalue = 0.02) (*P*,*P*,*M*)-***C*$_2$-3**. (c) 3DIMS maps and EDDB$_H$(r) plot (isovalue = 0.02) of (*M*,*M*,*P*)-***C*$_2$-4**. (d) 3DIMS maps and EDDB$_H$(r) plot (isovalue = 0.02) of (*P*,*P*,*M*)-***C*$_2$-5**. The calculated fraction of e per atom shown between parentheses corresponds to the % of delocalized π electrons in the molecule.

isotropy (AICD, an isotropic scalar criterion of aromaticity) with the ACID program[25] in cyclotris[5]helicene ***D*$_3$-3**, some of us previously showed that this macrocycle is, to some extent globally π-conjugated and exhibits triply twisted Möbius aromaticity.[7] Global Möbius aromaticity can *a priori* exist in both ***D*$_3$-3** (triply twisted) and ***C*$_2$-3** (singly twisted) as a consequence of the reduced torsion angle at the single bonds between the [5]helicene fragments, which allow ring-to-ring π delocalization.[5,9b] This can be verified in the DFT optimized geometries discussed above (see Tables S1 and S4 in the SI), and from single crystal X-ray diffraction data (SCXRD, see previously reported[7] data in CCDC 1826373 and 1826374): experimentally, in the monocrystalline racemate solid state, the average torsion angle is 30.1° (23.6–35.2°) in ***D*$_3$-3**, and 28.1° (15.2–40.2°) in ***C*$_2$-3**; it is significantly higher for biphenyl in the gas phase (44.4°).[26] The 3DIMS maps[10] of both ***D*$_3$-3** and ***C*$_2$-3** (Fig. 8) show only blue color, indicating an aromatic character of both molecules. The dark blue areas indicate intense delocalization, which is visibly occurring in each 22-electron semi-local circuits at each [5]helicene fragments. Now looking specially at the single bonds connecting the [5]helicene fragments, both maps allow to visualize the uninterrupted π conjugation across these single bonds: at all single bonds in ***D*$_3$-3** and ***C*$_2$-3**, and from any 3D perspective, a continuum of light blue color (and even medium blue color as revealed by close inspection, see the SI) between the C atoms is visible. The 3DIMS maps of ***D*$_3$-3** and ***C*$_2$-3** capture the chirality of their aromatic π systems and their twists. Detailed quantitative inspection revealed maximum IMS values over these bonds of 9.7 and 11.6 ppm (internal and external faces, respectively) for ***D*$_3$-3**, and 9.3 and 12.2 ppm (internal and external faces, respectively) for ***C*$_2$-3**, comparable with the value for the single bond in s-*cis*-butadiene (11.0 ppm),[10] the archetype of a π conjugated molecule. The $EDDB_H(r)$ analysis[11] of both ***D*$_3$-3** and ***C*$_2$-3** (Fig. 8) also confirmed their global Möbius aromatic character, with the delocalization of their π electrons extending to 76.0%, a value comparable to the one found in large kata-condensed isomeric [*n*]fibonacene tetraesters (*n* = 9–14).[27]

Comparison of the 3DIMS maps of ***C*$_2$-3** with the 3DIMS maps of its phenyl-tethered and alkyne-tethered analogues ***C*$_2$-4** [2f] (Fig. 8c) and ***C*$_2$-5** [2d] (Fig. 8d), respectively, is informative. As for ***C*$_2$-3**, the 3DIMS maps of ***C*$_2$-4** and ***C*$_2$-5** show only blue color, indicating they all are aromatic molecules. However, while the global conjugation in ***C*$_2$-3** and ***C*$_2$-4** can be visualized by a continuum of light blue or medium blue color over its single bonds in their 3DIMS map (indicating IMS ≥ 5.5 ppm over these bonds), the 3DIMS map of ***C*$_2$-5** shows visible areas of the neutral color over the alkynyl–[5]helicenyl single bonds (indicating IMS < 5.5 ppm over these bonds, see red arrows in Fig. 8d). This indicates that global π conjugation is significantly reduced at the alkyne tethers in ***C*$_2$-5**, when compared to the biphenyl-type single bonds in its analogs ***C*$_2$-3** and ***C*$_2$-4**. Just by a qualitative visual inspection, the 3DIMS maps in Fig. 8 indicate (i) that intense semi-local 22-electron circuits exist at each [5]helicene fragment in ***D*$_3$-3**, ***C*$_2$-3**, ***C*$_2$-4** and ***C*$_2$-5**, (ii) that significant yet less intense global π delocalization circuit exists in ***D*$_3$-3**, ***C*$_2$-3** and ***C*$_2$-4**, and (iii) that global π delocalization is weaker in ***C*$_2$-5**. In agreement with the 3DIMS analysis, the $EDDB_H(r)$ analysis of ***C*$_2$-5** indicated that only 70.9% of its π electrons are delocalized, while this fraction raises to 76.0% in both ***D*$_3$-3** and ***C*$_2$-3**, and is up to 80.3% in ***C*$_2$-4** (see Fig. S13 in the SI for the complementary analysis of ***D*$_3$-4**).

Conclusions

This article summarizes the comprehensive studies performed in our laboratories on the properties of the structurally appealing, yet stereochemically different, diastereomeric triply and singly twisted Möbius-shaped cyclotris[5]helicenes ***D*$_3$-3** and ***C*$_2$-3**. Their vibrational and electronic properties have been comprehensively examined experimentally by precision spectroscopies, with a focus on the tiny differences observed in their circularly polarized infrared, absorption and luminescence spectra. All experimentally observed spectroscopic responses (using or not circularly polarized light) could be suitably modeled and rationalized using DFT calculations. Additionally, DFT calculations allowed to examine comparatively their aromaticity (not an experimentally measurable property), including at the T_1 excited states in correlation with their phosphorescence. Detailed information could be obtained on the S_0, S_1 and T_1 electronic states of both diastereomeric molecules. This in-depth study on the properties of two stereochemically different semi-condensed π-conjugated macrocycles made of [5]helicene fragments shows that the differences in these diastereomeric molecules can be evidenced by several experimental and theoretical precision techniques.

Some highlights of this comprehensive study are: (i) the understanding that the enantiomerization process of ***C*$_2$-3** requires the inversion of configuration of a single [5]helicene fragment in a molecule that contains three [5]helicene fragments, and the demonstrated persistent chirality of ***D*$_3$-3**; (ii) the necessity to include dispersion correction schemes [D3 (BJ), preferably D4] in the DFT calculations to simulate accurately some properties (conformational and electronic) in this series; (iii) the demonstration of existing global π-electrons delocalization in these molecules as deduced from their experimental absorption and emission spectroscopies (including phosphorescence) and the theoretical evaluation of their aromaticity by advanced methods, thereby confirming their Möbius aromatic character; (iv) the relatively high fluorescence dissymmetry factor ($|g_{lum}| \geq 1.5 \times 10^{-3}$) and CPL brightness ($B_{CPL} \geq 2.4\ M^{-1}\ cm^{-1}$) for both macrocycles.

Overall, from the two examples thoroughly analyzed in this study and the previously analyzed examples, it becomes clear that semi-condensed π conjugated molecules made of [5]helicene fragments can exhibit global π electronic delocalization despite the presence of $C(sp^2)$–$C(sp^2)$ single bonds connecting their polycyclic π-conjugated systems, providing the torsion around these single bonds is restricted to ≤30°.

Author contributions

HB and FD performed the syntheses. NV performed the analytical and preparative resolution of the enantiomers by HPLC, the measurement of the barrier to enantiomerization of C_2-**3**, and the optical rotation dispersion measurements. JVN and YCo performed the theoretical conformational analyses. JVN performed the VCD and ECD analyses and related calculations. MR and LF performed the luminescence measurements, and DHR and YCa performed the corresponding calculations. AA performed the aromaticity analyses. FD and YCo conceived the study and obtained the research funds to realize it. YCo drafted the manuscript with revisions from all authors.

Conflicts of interest

There are no conflicts to declare.

Data availability

The data supporting this article have been included as part of the supplementary information (SI). All analytical raw data (spectroscopy data and the corresponding DFT simulations) are available upon reasonable request to the authors (FD and YCo).

Supplementary information: all details of the studies and complementary data (PDF), all 3DIMS maps discussed herein (VTK). See DOI: **https://doi.org/10.1039/d5qo01741f**.

Acknowledgements

This work was funded in part by the French Agence Nationale de la Recherche—ANR (ANR-13-JS07-0009 and ANR-19-CE07-0041) and the German Research Foundation (SFB677). This work was supported by the computing facilities of the Centre Régional de Compétences en Modélisation Moléculaire de Marseille—CRCMM. Institutional financial support from Aix Marseille University, University of Bordeaux, University of Rennes, Centrale Méditerranée and the Centre National de la Recherche Scientifique—CNRS is gratefully acknowledged.

References

1 (*a*) E. Clar, C. T. Ironside and M. Zander, The electronic interaction between benzenoid rings in condensed aromatic hydrocarbons. 1:12-2:3-4:5-6:7-8:9-10:11-hexabenzocoronene, 1:2-3:4-5:6-10:11-tetrabenzoanthanthrene, and 4:5-6:7-11:12-13:14-tetrabenzoperopyrene, *J. Chem. Soc.*, 1959, 142, DOI: **10.1039/JR9590000142**; (*b*) L. Barnett, D. M. Ho, K. K. Baldridge and R. A. Pascal Jr., The Structure of Hexabenzotriphenylene and the Problem of Overcrowded "D_{3h}" Polycyclic Aromatic Compounds, *J. Am. Chem. Soc.*, 1999, **121**, 727, DOI: **10.1021/ja983471i**; (*c*) D. Peña, D. Pérez, E. Guitián and L. Castedo, Synthesis of Hexabenzotriphenylene and Other Strained Polycyclic Aromatic Hydrocarbons by Palladium-Catalyzed Cyclotrimerization of Arynes, *Org. Lett.*, 1999, **1**, 1555, DOI: **10.1021/ol990864t**; (*d*) D. Peña, A. Cobas, D. Pérez, E. Guitián and L. Castedo, Kinetic Control in the Palladium-Catalyzed Synthesis of C_2-Symmetric Hexabenzotriphenylene. A Conformational Study, *Org. Lett.*, 2000, **2**, 1629, DOI: **10.1021/ol005916p**; (*e*) H. Kashihara, T. Asada and K. Kamikawa, Synthesis of a Double Helicene by a Palladium-Catalyzed Cross-Coupling Reaction: Structure and Physical Properties, *Chem. – Eur. J.*, 2015, **21**, 6523, DOI: **10.1002/chem.201500074**; (*f*) H. Saito, A. Uchida and S. Watanabe, Synthesis of a Three-Bladed Propeller-Shaped Triple [5]Helicene, *J. Org. Chem.*, 2017, **82**, 5663, DOI: **10.1021/acs.joc.7b00486**; (*g*) T. Hosokawa, Y. Takahashi, T. Matsushima, S. Watanabe, S. Kikkawa, I. Azumaya, A. Tsurusaki and K. Kamikawa, Synthesis, Structures, and Properties of Hexapole Helicenes: Assembling Six [5]Helicene Substructures into Highly Twisted Aromatic Systems, *J. Am. Chem. Soc.*, 2017, **139**, 18512, DOI: **10.1021/jacs.7b07113**; (*h*) V. Berezhnaia, M. Roy, N. Vanthuyne, M. Villa, J.-V. Naubron, J. Rodriguez, Y. Coquerel and M. Gingras, Chiral Nanographene Propeller Embedding Six Enantiomerically Stable [5] Helicene Units, *J. Am. Chem. Soc.*, 2017, **139**, 18508, DOI: **10.1021/jacs.7b07622**; (*i*) A. Artigas, M. A. Ortuño, J. Castro-Esteban, M. Giorgi, D. Peña, D. Pérez and Y. Coquerel, Water-Mediated 1,7-Palladium Aryl-to-Aryl Migration in an Unusual Aryne Trimerization Enables the Synthesis of Multihelicenes with Profoundly Hindered Stereogenic Axes, *Adv. Synth. Catal.*, 2025, **367**, e202500338, DOI: **10.1002/adsc.202500338**.

2 (*a*) B. Thulin and O. Wennerström, Propellicene or Bi-2,13-pentahelicenylene, *Acta Chem. Scand., Ser. B*, 1976, **30**, 688; (*b*) T. Matsushima, S. Kikkawa, I. Azumaya and S. Watanabe, Triple Helicene Cage: Three-Dimensional π-Conjugated Chiral Cage with Six [5]Helicene Units, *ChemistryOpen*, 2018, **7**, 278, DOI: **10.1002/open.201800006**; (*c*) H. Kubo, D. Shimizu, T. Hirose and K. Matsuda, Circularly Polarized Luminescence Designed from Molecular Orbitals: A Figure-Eight-Shaped [5]Helicene Dimer with D_2 Symmetry, *Org. Lett.*, 2020, **22**, 9276, DOI: **10.1021/acs.orglett.0c03506**; (*d*) X. Jiang, J. D. Laffoon, D. Chen, S. Pérez-Estrada, A. S. Danis, J. Rodríguez-López, M. A. Garcia-Garibay, J. Zhu and J. S. Moore, Kinetic Control in the Synthesis of a Möbius Tris((ethynyl)[5]helicene) Macrocycle Using Alkyne Metathesis, *J. Am. Chem. Soc.*, 2020, **142**, 6493, DOI: **10.1021/jacs.0c01430**; (*e*) V. Houska, E. Ukraintsev, J. Vacek, J. Rybáček, L. Bednárová, R. Pohl, I. G. Stará, B. Rezek and I. Starý, Helicene-based π-conjugated macrocycles: their synthesis, properties, chirality and self-assembly into molecular stripes on a graphite surface, *Nanoscale*, 2023, **15**, 1542, DOI: **10.1039/D2NR04209F**; (*f*) Q. Zhou, W. Yuan, Y. Li,

Y. Han, L. Bao, W. Fan, L. Jiao, Y. Zhao, Y. Ni, Y. Zou, H.-B. Yang and J. Wu, [5]Helicene Based π-Conjugated Macrocycles with Persistent Figure-Eight and Möbius Shapes: Efficient Synthesis, Chiral Resolution and Bright Circularly Polarized Luminescence, *Angew. Chem., Int. Ed.*, 2025, **64**, e202417749, DOI: **10.1002/anie.202417749**.

3 L. Sturm, F. Aribot, L. Soliman, H. Bock and F. Durola, The Perkin Strategy for the Synthesis of Large Carboxy-Substituted Polycyclic Aromatic Compounds, *Eur. J. Org. Chem.*, 2022, e202200196, DOI: **10.1002/ejoc.202200196**.

4 A. Robert, P. Dechambenoit, E. A. Hillard, H. Bock and F. Durola, Non-planar oligoarylene macrocycles from biphenyl, *Chem. Commun.*, 2017, **53**, 11540, DOI: **10.1039/C7CC06798D**.

5 F. Aribot, A. Merle, P. Dechambenoit, H. Bock, A. Artigas, N. Vanthuyne, Y. Carissan, D. Hagebaum-Reignier, Y. Coquerel and F. Durola, A Triply [5]Helicene-Bridged (1,3,5)Cyclophane, *Angew. Chem., Int. Ed.*, 2023, **62**, e202304058, DOI: **10.1002/anie.202304058**.

6 (*a*) T. Kawase and M. Oda, Möbius Aromatic Hydrocarbons: Challenges for Theory and Synthesis, *Angew. Chem., Int. Ed.*, 2004, **43**, 4396, DOI: **10.1002/anie.200460050**; (*b*) H. S. Rzepa, Möbius Aromaticity and Delocalization, *Chem. Rev.*, 2005, **105**, 3697, DOI: **10.1021/cr030092l**; (*c*) R. Herges, Topology in Chemistry: Designing Möbius Molecules, *Chem. Rev.*, 2006, **106**, 4820, DOI: **10.1021/cr0505425**.

7 G. Naulet, L. Sturm, A. Robert, P. Dechambenoit, F. Röhricht, R. Herges, H. Bock and F. Durola, Cyclic tris-[5]helicenes with single and triple twisted Möbius topologies and Möbius aromaticity, *Chem. Sci.*, 2018, **9**, 8930, DOI: **10.1039/C8SC02877J**.

8 A. Robert, G. Naulet, H. Bock, N. Vanthuyne, M. Jean, M. Giorgi, Y. Carissan, C. Aroulanda, A. Scalabre, E. Pouget, F. Durola and Y. Coquerel, Cyclobishelicenes: Shape-Persistent Figure-Eight Aromatic Molecules with Promising Chiroptical Properties, *Chem. – Eur. J.*, 2019, **25**, 14364, DOI: **10.1002/chem.201902637**.

9 (*a*) M. Orozco-Ic, L. Soriano-Agueda, S. Escayola, D. Sundholm, G. Merino and E. Matito, Understanding Aromaticity in [5]Helicene-Bridged Cyclophanes: A Comprehensive Study, *J. Org. Chem.*, 2024, **89**, 2459, DOI: **10.1021/acs.joc.3c02485**; (*b*) A. Artigas, Y. Carissan, D. Hagebaum-Reignier, H. Bock, F. Durola and Y. Coquerel, Aromaticity in Semi-Condensed Figure-Eight Molecules, *Chem. – Eur. J.*, 2024, e202401016, DOI: **10.1002/chem.202401016**.

10 A. Artigas, D. Hagebaum-Reignier, Y. Carissan and Y. Coquerel, Visualizing electron delocalization in contorted polycyclic aromatic hydrocarbons, *Chem. Sci.*, 2021, **12**, 13092, DOI: **10.1039/D1SC03368A**.

11 D. W. Szczepanik, M. Andrzejak, J. Dominikowska, B. Pawelek, T. M. Krygowski, G. Szatylowicz and M. Solà, The electron density of delocalized bonds (EDDB) applied for quantifying aromaticity, *Phys. Chem. Chem. Phys.*, 2017, **19**, 28970, DOI: **10.1039/C7CP06114E**.

12 Reviews: (*a*) W. R. Kitzmann, J. Freudenthal, A.-P. M. Reponen, Z. A. VanOrman and S. Feldmann, Fundamentals, Advances, and Artifacts in Circularly Polarized Luminescence (CPL) Spectroscopy, *Adv. Mater.*, 2023, **35**, 2302279, DOI: **10.1002/adma.202302279**; (*b*) M. Cei, L. Di Bari and F. Zinna, Circularly polarized luminescence of helicenes: A data-informed insight, *Chirality*, 2023, **35**, 192, DOI: **10.1002/chir.23535**; (*c*) M. Hasegawa, Y. Nojima and Y. Mazaki, Circularly Polarized Luminescence in Chiral π-Conjugated Macrocycles, *ChemPhotoChem*, 2021, **5**, 1042, DOI: **10.1002/cptc.202100162**; (*d*) T. Mori, Chiroptical Properties of Symmetric Double, Triple, and Multiple Helicenes, *Chem. Rev.*, 2021, **121**, 2373, DOI: **10.1021/acs.chemrev.0c01017**; (*e*) V. Kumar, J. L. Páez, S. Míguez-Lago, J. M. Cuerva, C. M. Cruz and A. G. Campaña, Chiral nanographenes exhibiting circularly polarized luminescence, *Chem. Soc. Rev.*, 2025, **54**, 4922, DOI: **10.1039/D4CS00745J**.

13 (*a*) J. Wade, J. R. Brandt, D. Reger, F. Zinna, K. Y. Amsharov, N. Jux, D. L. Andrews and M. Fuchter, 500-Fold Amplification of Small Molecule Circularly Polarised Luminescence through Circularly Polarised FRET, *Angew. Chem., Int. Ed.*, 2021, **60**, 222, DOI: **10.1002/anie.202011745**; (*b*) L. E. M. White, T.-M. Gianga, F. Pradaux-Caggiano, C. Faverio, A. Taddeucci, H. S. Rzepa, C. Jonhannesen, L. E. Hatcher, G. Siligardi, D. R. Carbery and G. Dan Santos, Enantiopure synthesis of [5]helicene based molecular lemniscates and their use in chiroptical materials, *Nat. Commun.*, 2025, **16**, 2837, DOI: **10.1038/s41467-025-58162-1**; (*c*) Y. Deng, M. Wang, Y. Zhuang, S. Liu, W. Huang and Q. Zhao, Circularly polarized luminescence from organic micro-/nano-structures, *Light: Sci. Appl.*, 2021, **10**, 76, DOI: **10.1038/s41377-021-00516-7**; (*d*) C. Yin, S. Sun, Z.-A. Yan, H. Hu, P. Jiang, Z. Xu, H. Tian and X. Ma, A universal strategy for multicolor organic circularly polarized afterglow materials with high dissymmetry factors, *Proc. Natl. Acad. Sci. U. S. A.*, 2025, **122**, e2419481122, DOI: **10.1073/pnas.2419481122**; (*e*) S. Liu, X. Liu, Y. Wu, D. Zhang, Y. Wu, H. Tian, Z. Zheng and W.-H. Zhu, Circularly polarized perovskite luminescence with dissymmetry factor up to 1.9 by soft helix bilayer device, *Matter*, 2022, **5**, 2319, DOI: **10.1016/j.matt.2022.05.012**; (*f*) X. Hao, Z. Chen, H. Ma, Y. Wang, Y. Cao, B. Yao, R. Wang, R. Cao, Y. Xiao, C. Liu, Y. Liu, S. Feng, H. Dai, X.-D. Zhang and Y.-J. Liu, Dual-band high-dissymmetry circularly polarized luminescence from cholesteric liquid crystals overlaid a gold cluster film, *Nat. Commun.*, 2025, **16**, 9639, DOI: **10.1038/s41467-025-64637-y**; (*g*) S. Huang, Q. Wu, M. Zhou, Y. Wen, Y. Yuan and H. Zhang, Photothermal-responsive chiral liquid crystal copolymers with tunable circularly polarized luminescence and a maximum g_{lum} of 1.95, *Mater. Today Chem.*, 2025, **47**, 102878, DOI: **10.1016/j.mtchem.2025.102878**.

14 (*a*) S. Grimme, J. Antony, S. Ehrlich and H. Krieg, A consistent and accurate *ab initio* parametrization of density functional dispersion correction (DFT-D) for the 94 elements

H-Pu, *J. Chem. Phys.*, 2010, **132**, 154104, DOI: 10.1063/1.3382344; (*b*) S. Grimme, S. Ehrlich and L. Goerigk, Effect of the damping function in dispersion corrected density functional theory, *J. Comput. Chem.*, 2011, **32**, 1456, DOI: 10.1002/jcc.21759.

15 C. Goedicke and H. Stegemeyer, Resolution and racemization of pentahelicene, *Tetrahedron Lett.*, 1970, **12**, 937, DOI: 10.1016/S0040-4039(01)97871-2.

16 H. Tanaka, M. Ikenosako, Y. Kato, M. Fujiki, Y. Inoue and T. Mori, Symmetry-based rational design for boosting chiroptical responses, *Commun. Chem.*, 2018, **1**, 38 https://www.nature.com/articles/s42004-018-0035-x.

17 Y. Nakai, T. Mori and Y. Inoue, Theoretical and Experimental Studies on Circular Dichroism of Carbo[*n*]helicenes, *J. Phys. Chem. A*, 2012, **116**, 7372, DOI: 10.1021/jp304576g.

18 (*a*) M. Sapir and E. Vander Donckt, Intersystem crossing in the helicenes, *Chem. Phys. Lett.*, 1975, **36**, 108, DOI: 10.1016/0009-2614(75)85698-3; (*b*) N. I. Nijegorodov and W. S. Downey, The Influence of Planarity and Rigidity on the Absorption and Fluorescence Parameters and Intersystem Crossing Rate Constant in Aromatic Molecules, *J. Phys. Chem.*, 1994, **98**, 5639, DOI: 10.1021/j100073a011; (*c*) K. Nagarajan, A. R. Mallia, K. Muraleedharan and M. Hariharan, Enhanced intersystem crossing in core-twisted aromatics, *Chem. Sci.*, 2017, **8**, 1776, DOI: 10.1039/C6SC05126J.

19 B. de Souza, G. Farias, F. Neese and R. Izsák, Predicting Phosphorescence Rates of Light Organic Molecules Using Time-Dependent Density Functional Theory and the Path Integral Approach to Dynamics, *J. Chem. Theory Comput.*, 2019, **15**, 1896, DOI: 10.1021/acs.jctc.8b00841.

20 F. Neese, The ORCA program system, *Wiley Interdiscip. Rev.: Comput. Mol. Sci.*, 2012, **2**, 73, DOI: 10.1002/wcms.81.

21 E. Caldeweyher, C. Bannwarth and S. Grimme, Extension of the D3 dispersion coefficient model, *J. Chem. Phys.*, 2017, **147**, 034112, DOI: 10.1063/1.4993215.

22 T. Kato, D. Imoto, A. Yagi and K. Itami, Making non-emissive [6]cycloparaphenylene fluorescent by simple multiple methyl substitution, *Chem. Sci.*, 2025, **16**, 18952, DOI: 10.1039/D5SC04694G.

23 L. Arrico, L. Di Bari and F. Zinna, Quantifying the Overall Efficiency of Circularly Polarized Emitters, *Chem. – Eur. J.*, 2021, **27**, 2920, DOI: 10.1002/chem.202002791.

24 A. Artigas, N. Ferdi, M. Rémond, F. Rigoulet, N. Vanthuyne, D. Hagebaum-Reignier, Y. Carissan, J.-V. Naubron, M. Giorgi, L. Favereau and Y. Coquerel, Conformational, Structural, and Chiroptical Properties of an Overcrowded Triply Fused Carbo[7]helicene, *J. Org. Chem.*, 2024, **89**, 498, DOI: 10.1021/acs.joc.3c02239.

25 D. Geuenich, K. Hess, F. Köhler and R. Herges, Anisotropy of the Induced Current Density (ACID), a General Method To Quantify and Visualize Electronic Delocalization, *Chem. Rev.*, 2005, **105**, 3758, DOI: 10.1021/cr0300901.

26 A. Almenningen, O. Bastiansen, L. Fernholt, B. N. Cyvin, S. J. Cyvin and S. Samdal, Structure and barrier of internal rotation of biphenyl derivatives in the gaseous state: Part 1. The molecular structure and normal coordinate analysis of normal biphenyl and pedeuterated biphenyl, *J. Mol. Struct.*, 1985, **128**, 59, DOI: 10.1016/0022-2860(85)85041-9.

27 L. Sturm, A. Artigas, Y. Coquerel, I. H. Bechtold, F. Durola and H. Bock, Helicene Aromaticity Deviates from the Clar Rule—On the Electronic Dissimilarity of Large Isomeric Fibonacenes, *Angew. Chem., Int. Ed.*, 2024, **63**, e202403170, DOI: 10.1002/anie.202403170.

